The Influence of the Molecular Weight on the Thermotropic Alignment and Self-Organized Structure Formation of Branched Side Chain Hairy-Rod Polyfluorene in Thin Films

Matti Knaapila,*,† Roman Stepanyan,‡ Benjamin P. Lyons,† Mika Torkkeli,§ Thomas P. A. Hase,† Ritva Serimaa,§ Roland Güntner,⊥ Oliver H. Seeck,#,▽ Ullrich Scherf,⊥ and Andrew P. Monkman†

Department of Physics, University of Durham, South Road, Durham DH1 3LE, United Kingdom; Department of Applied Physics, University of Twente, P.O. Box 217, 7500 AE Enschede, The Netherlands; Department of Physical Sciences, P.O. Box 64, FI-00014, University of Helsinki, Helsinki, Finland; Makromolekulare Chemie and Institut für Polymertechnologie, Bergische Universität Wuppertal, D-42097 Wuppertal, Germany; and Institut für Festkörperforschung, Forschungszentrum Jülich GmbH, D-52425 Jülich, Germany

Received November 3, 2004; Revised Manuscript Received January 14, 2005

ABSTRACT: We report on the influence of the molecular weight (M_n) on the alignment and structure of poly(9,9-bis(ethylhexyl)fluorene-2,7-diyl) (PF2/6) in thin films on rubbed polyimide in the equilibrium. The degree of alignment has been studied using optical spectroscopy and compared to theoretical arguments. The structure of PF2/6 has been studied using grazing-incidence X-ray diffraction. PF2/6 realizes a threshold molecular weight $M_n^* = 10^4$ g/mol separating a low M_n (LMW, $M_n < M_n^*$) and a high M_n (HMW, $M_n > M_n^*$) region. LMW materials show only the nematic (Nem) phase while HMW compounds show hexagonal (Hex) and Nem phases at low and high temperatures, respectively. LMW samples align equally well at any temperature above the glass transition, and the dichroic ratio, R, increases with M_n. HMW material aligns well in the Nem regime, and R drops exponentially with M_n, which is in agreement with the theory. The orientational order is maximized near M_n^*, and the orientational order parameter is >0.9. HMW samples, whether aligned or not, reveal two kinds of coexistent Hex crystallites distributed in the sample plane having one crystal axis **a** perpendicular or parallel to the surface. Local order within the triaxially aligned Hex phase surpasses that of the in-plane aligned Hex phase.

I. Introduction

The design of mesomorphic structures[1] and thin films[2,3] coupled with an understanding of the nanoscale structure−property relationships[4] is paramount in the research of π-conjugated polymers. These materials are hairy-rod polymers (see e.g. refs 5−7) consisting of a stiff backbone where a dense set of flexible side chains are bonded, resulting in self-organization. Especially poly(alkylthiophenes) (PATs)[8] are π-conjugated prime examples where hairy-rod structure leads to the self-organization[3] with enhanced electronic characteristics.[2]

Polyfluorenes (PFs)[9] are promising π-conjugated hairy rods for applications. They allow uniaxial alignment which yields emission of linearly polarized light in light-emitting diodes (LEDs)[10] and an enhanced mobility in thin-film transistors (TFTs).[11,12] Altogether their molecular structure,[9] self-organization,[13] overall alignment,[11] and larger scale morphology[14] combined with their thermal behavior[15] determine their performance and should be addressed in a concerted effort.

Besides the much studied linear side chain poly(9,9-(di-*n*,*n*-octyl)fluorene) (PF8), the branched side chain poly(9,9-bis(ethylhexyl)fluorene-2,7-diyl) (PF2/6)[9,16] is of particular interest. First, its simple structure and stability allow its straightforward use as a model molecule for phase behavior studies.[17] Second, its optoelectronic properties and facile alignment put forward its use in thin film devices. In general, PF2/6 takes a higher degree of alignment than PF8.[9]

PF2/6 has been found to form a hexagonal packing of 5-helical rigid molecules.[15,18,19] Polyimide (PI), which is a hairy rod itself,[20] is in turn a basic compound in PF2/6-based polarized LEDs.[21,22] The alignment of PFs on PI is known e.g. as a function of dopant concentration[23] or solvent.[24] PF2/6 chains run parallel to the substrate in the rubbing direction of PI, and PF2/6 shows two differently oriented coexisting crystalline structures in axially and in-plane aligned thin films[19] for high M_n PF2/6 ($M_n = 147$ kg/mol): A part of the crystallites have one crystal axis **a** perpendicular and a part parallel to the substrate surface. Multiple orientation in π-conjugated polymers has previously been found for poly(*p*-phenylenevinylene)[25] and poly(3-hexylthiophene).[2,3] The monoaxial distributions, "inverse combs", are reported for PATs.[26] A considerable increase in the degree of alignment[27,28] accompanied by the loss of order along the (ab0) plane[27] is seen for low M_n PF2/6 ($M_n = 8$ kg/mol).

Molecular weight (M_n) influences the self-organization of hairy rods such as poly(*p*-phenylene) (PPP).[29] The optoelectronic effect of M_n on PATs[30−32] has been studied. Papadopoulos et al.[33] reported the influence of M_n on the molecular dynamics and glass transition of PF8 and analogous oligomers. Banach et al.[34] studied the influence of M_n on thermotropic alignment of poly(9,9-dioctylfluorene-*co*-benzothiadiazole) (F8BT) on PI

† University of Durham.
‡ University of Twente.
§ University of Helsinki.
⊥ Bergische Universität Wuppertal.
Forschungszentrum Jülich GmbH.
▽ Also at HASYLAB am DESY, Notkestrasse 85, D-22605 Hamburg, Germany.
* Corresponding author: Tel +44-191-33-43558, Fax +44-191-33-43585, e-mail matti.knaapila@durham.ac.uk.

10.1021/ma0477403 CCC: $30.25
Published on Web 02/24/2005

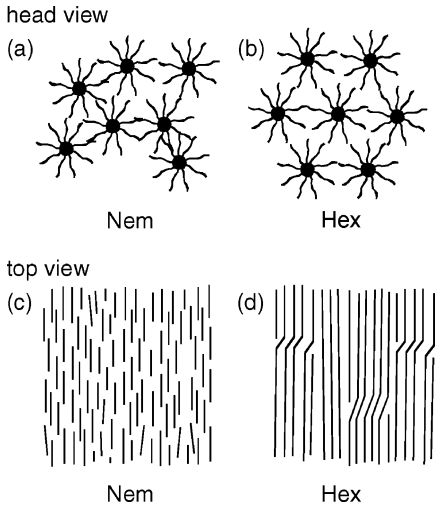

Figure 1. Self-organized nematic (Nem) and hexagonal (Hex) phase of hairy-rod polymers drawn end-on (a, b) and their uniaxially aligned structure drawn side on (c, d) (not to scale).

using M_n in the range 62−129 kg/mol. These authors found the highest alignment in lowest M_n films and concluded it to be limited by viscosity and the formation of a macroscopic multidomain structure. The alignment of long and short molecules has been described in the theory of nematic order by Khokhlov and Semenov.[35]

We have recently studied the phase behavior of PF2/6 in bulk as a function of M_n using a M_n range 3−150 kg/mol.[17] The phase diagram contains a glass transition (T_g) and a limit $M_n^* = 10^4$g/mol which define the boundary between a low M_n (LMW) region ($M_n < M_n^*$) for which only a nematic (Nem) phase is seen and a high M_n (HMW) region ($M_n > M_n^*$) for which hexagonal (Hex) and Nem phases are observed at low and high T, respectively. These phases are illustrated in Figure 1.

In this paper we report on the influence of M_n on the thermotropic alignment and self-organization of PF2/6 in thin films on rubbed PI. The alignment has been studied as a function of M_n using optical spectroscopy and compared to the theoretical predictions for static situation. The structure has been studied using grazing-incidence X-ray diffraction (GIXD). The phase diagram[17] has been employed to optimize the alignment conditions and structure in films. The similarities (phase domains) and differences (alignment and multiple orientation of crystallites) between bulk[17] and film are highlighted. Both the orientational and local order are maximized near the phase boundary $M_n^* = 10^4$ g/mol. These results form guidelines on how to use M_n as a tuning parameter of thermotropic alignment of PF2/6 in thin films.

II. Theoretical Section

Self-Organized Phases as a Function of Molecular Weight. Here we outline the theory used in refs 17 and 27 to describe the Nem−Hex transition and present a simple generalization to consider the uniaxial orientation (see Figure 2). The free energy of the Nem phase is given as[36,37]

$$F_N \approx k_B TVc \ln\left(\frac{f}{e}\right) + k_B TVc \ln\left(\frac{4\pi}{\Omega_N}\right) \qquad (1)$$

where the translational and orientational entropy are represented by the first and second terms, respectively. Here k_BT is a Boltzmann factor, V the volume of the sample, c the concentration of the molecules, f the volume fraction of the backbone, and e the Euler number. The quantity Ω_N describes the degree of overall (uniaxial) alignment: the smaller it is, the more aligned is the system.

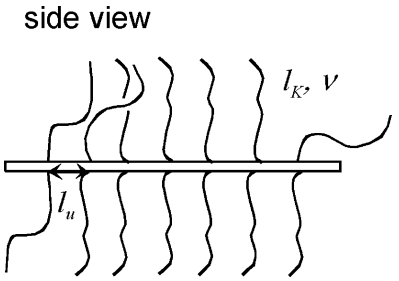

Figure 2. A hairy-rod-like polymer of rigid backbone and flexible side chains. l_K and ν are the segment length (the Kuhn length) and the segment volume of the side chains; l_u is the distance between grafting points (the unit length) of the backbone.

The Hex phase reveals negligible translational entropy, and the interaction between ordered molecules becomes dominant. This interaction arises from the inhomogeneous side chain ends distribution. For hairy rods it reads with accuracy up to a numerical prefactor

$$F_{lattice} \approx -k_B TV \frac{\nu}{\nu_0 l_K^2 l_u} \qquad (2)$$

where ν is the volume and l_K the Kuhn length of one chain segment, l_u the distance between two consecutive grafting points, i.e., the length of the repeat unit, and ν_0 the volume of one repeat unit of the hairy rod. From eq 2 the free energy of the hexagonally ordered material is obtained as

$$F_H \approx k_B TVc \ln\left(\frac{4\pi}{\Omega_H}\right) - k_B TV \frac{\nu}{\nu_0 l_K^2 l_u} \qquad (3)$$

Because of incompressibility, the concentration $c = M_u/(\nu_0 M_n)$, where M_n and M_u are the molecular weights of a polymer and one repeat unit, respectively, is directly related to M_n. Equations 1 and 3 imply that the higher the M_n, the more favorable the Hex packing. The value of M_n separating Nem and Hex phases for given parameters, M_n^*, is

$$M_n^* \approx M_u \frac{l_K^2 l_u}{\nu} \ln\left(\frac{e\Omega_N}{f\Omega_H}\right) \qquad (4)$$

Overall Alignment. Both phases have been previously assumed to be "equally aligned", i.e. $\Omega_N \simeq \Omega_H$,[27] which holds only for the temperatures not far from T_g. In contrast, here we consider the binodal including the orientational part. When the details of the orientation have been omitted, both phases are assumed relatively highly aligned (cf. the discussion of the measured alignment in section IV). In general, a quite sophisticated theoretical treatment should be applied to reveal the features of the alignment in the hairy-rod system; see for instance refs 5−7. Nevertheless, the temperature and M_n dependence can be estimated by a simple argument. The polymer consists of stiff segments with a certain Kuhn length l_K^{HR} where the superscript HR stands for "hairy rod" . In the aligned state (Nem or Hex)

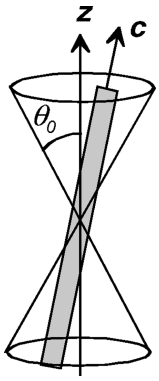

Figure 3. Illustration of the alignment. The vectors **z** and **c** represent the alignment direction and the backbone of the molecule, respectively.

at low temperature the direction of each segment can fluctuate in the solid angle as[38,39]

$$\Omega_0 \approx \frac{d}{l_K^{HR}} \tag{5}$$

where d is the diameter of the backbone (see Figure 3). Apparently, when the temperature increases, Ω_0 is also increased. A rough first-order approximation of Ω_0 is expressed as

$$\Omega_0 \approx \frac{d}{l_K^{HR}}(1 + Ct) \tag{6}$$

where C is a phenomenological constant probably different for different phases and where $t = T - T_g$ is the temperature measured from the T_g. If the Kuhn segments are treated independently, the total configurational space accessible for fluctuations of the chain is

$$\Omega_i(t) \approx \left(\frac{d}{l_K^{HR}}(1 + C_i t)\right)^{M_n l_u / M_u l_K^{HR}} \tag{7}$$

where i = N, H refers to "Nem" or "Hex" , respectively. This allows us to estimate the ratio

$$\frac{\Omega_N(t)}{\Omega_H(t)} \approx \left(\frac{1 + C_N t}{1 + C_H t}\right)^{M_n l_u / M_u l_K^{HR}} \tag{8}$$

Then, the eqs 4 and 8 yield the equation for T vs M_n binodal. When linearized for t we get

$$t \approx A\left(1 - \frac{M_{n0}^*}{M_n^*}\right) \tag{9}$$

where

$$M_{n0}^* \approx M_u \frac{l_K^2 l_u}{\nu} \ln\left(\frac{e}{f}\right) \tag{10}$$

and where $A = \ln(e/f) l_K^{HR}/(l_u(C_N - C_H)/M_{n0}^*)$. A incorporates both phenomenological constants C_N and C_H and is the only adjustable parameter of the treatment.

Next, we clarify what Ω means in terms of the order parameter s (cf. e.g. ref 40). The molecule, whose rigid backbone is defined by the vector **c**, is free to rotate in the solid angle Ω so that it can take any orientation with angle θ with the director between 0 and θ_0, where $\Omega = 4\pi(1 - \cos\theta_0)$ (cf. Figure 3). In the ordered state

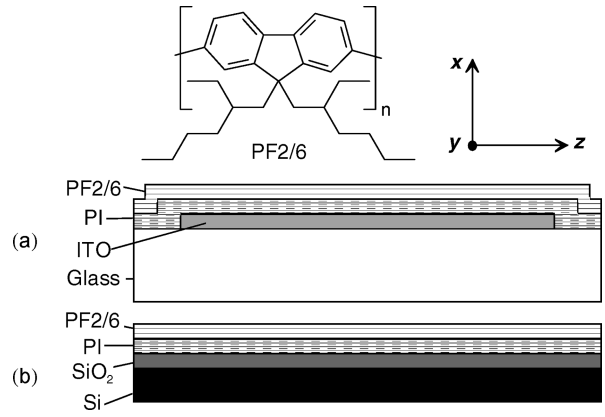

Figure 4. Formula of poly(9,9-bis(ethylhexyl)-2,7-diyl) (PF2/6) and the side views of differently prepared PF2/6 samples either on (a) glass/ITO or (b) Si/SiO_2 substrates. The vectors **x**, **y**, and **z** define the surface normal and the directions perpendicular and parallel to the orientation direction in-plane, respectively (cf. Figure 3).

the angular distribution function $f(\theta)$ can be approximated as

$$f(\theta) = \begin{cases} \tilde{c}, & \text{if } 0 < \theta < \theta_0 \text{ or } \pi - \theta_0 < \theta < \pi \\ 0 & \text{otherwise} \end{cases} \tag{11}$$

The constant $\tilde{c}$ is found from the normalization of f and is $\tilde{c} = 0.5/(1 - \cos\theta_0)$. The order parameter s and the angle Ω are in turn

$$s = \int_0^\pi \mathrm{d}\theta\, f(\theta) \frac{3\cos^2\theta - 1}{2} = \frac{1}{2}\left(1 - \frac{\Omega}{4\pi}\right)\left(2 - \frac{\Omega}{4\pi}\right) \tag{12}$$

$$\frac{\Omega}{4\pi} = \frac{3 - \sqrt{1 + 8s}}{2} \tag{13}$$

Here $s = 0$ and $s = 1$ respectively correspond to prefect freedom and alignment with $\Omega = 4\pi$ and $\Omega = 0$.

The order parameter is related to the dichroic ratio for absorption, which is defined as

$$R = |\bar{E}_{||}/\bar{E}_{\perp}| \tag{14}$$

where $\bar{E}_{||}$ and $\bar{E}_{\perp}$ are the maximum values of the absorbance for light polarized parallel and perpendicular to the alignment direction **z** and potentially parallel to the molecular **c** axis (cf. Figure 3). R describes the anisotropy of the absorption process. The transition probability is maximized when the transition moment of the molecule lies parallel to the electric vector of the light. The transition moment is assumed to be parallel to the **c** axis. R is related to the order parameter as $s = (R - 1)/(R + 2)$. Therefore, for large R, eq 13 implies

$$\frac{\Omega}{4\pi} \approx \frac{2}{R} + O(R^{-2}) \tag{15}$$

In particular, we see that if Ω increases exponentially with M_n, as eq 7, then R decreases also exponentially. To make a difference between the order occurring at intermolecular self-organization and overall orientation, we denote the first one as "local" order.

III. Experimental Section

Materials and Alignment. The preparation of PF2/6[9,21] (Figure 4) has been described elsewhere. Six different M_n's

Table 1. Molecular Characteristics of the PF2/6 Samples

material	M_n (g/mol)	M_w (g/mol)
3/5-PF2/6	2 900	4 800
8/15-PF2/6	7 600	15 000
29/68-PF2/6	29 000	68 000
62/138-PF2/6	62 000	138 000
92/190-PF2/6	91 500	190 000
147/260-PF2/6	~147 000	~262 000

were used and determined using GPC (Table 1). The samples are denoted henceforth as $(M_n/M_w)10^{-3}$-PF2/6. The third sample type had an *N*-di(4-methylphenyl)aminophenyl end cap while the first two were phenyl end-capped. The polymers were dissolved in a 3:1 mixture of toluene and chloroform (Aldrich). Two parallel sample series were made by spin-coating from 10 mg/mL solutions at 2500 rpm for 60 s under clean room conditions. The substrates were quartz (Spectrosil quartz disks of Saint-Gobain Quartz Plc) and pretreated PI substrates (LCD cells obtained from E.H.C. Co. Ltd., Japan, and split open for this purpose (Figure 4a)). Thicknesses of PI, indium tin oxide (ITO), and glass of LCDs were around 100 nm, 30 nm, and 1 mm, respectively. To provide yet another parallel experiment for comparison, pretreated Si/SiO_2/PI substrates were employed (Figure 4b). They were Si/SiO_2 substrates where the SiO_2 layers were formed on the silicon by wet thermal oxidation. This technique involves baking wafers in a furnace through which water vapor is passed. Initially, an oxide grows on the surface and then diffuses inward. This oxide was then etched back using buffered hydrofluoric acid to achieve the desired thickness. The oriented PI layers were prepared adapting the method from ref 21. The PI precursor (Merck KG) was spun onto the wafer at 2500 rpm and then heated at 85 °C for 20 min in air to remove any residual solvent. This was followed by heating for 40 min at 300 °C in vacuo, after which the film was allowed to cool. The layer was then rubbed uniaxially using a rayon cloth. The thickness of SiO_2 and PI was known from ellipsometric measurements; SiO_2 varied from 10 to 140 nm, and that of the PI layer had a mean thickness of 34 ± 3 nm. All the samples were subsequently annealed under argon either at 80 °C for 10 min or at 180 °C either for 3 or 18 h and cooled at a rate of 3 °C/min. Both the bulk polymer and all samples were stored under nitrogen or helium and/or in dark or under yellow light to prevent any photooxidation prior to or during measurements.

Optical Measurements. Polarized absorption measurements were made using a JA Woollam & Co. VASE ellipsometer with built-in polarizers, set up in transmission mode. A bare PI substrate was used as a reference. To calculate the dichroic ratio in absorption for each of the aligned samples, transmission spectra were measured for light polarized parallel and perpendicular to the alignment direction. The transmission spectra were then converted to absorption spectra via $E = -\log(T)$, where E is the optical density and T is the transmission of the sample. The absorption spectrum of each sample was compared to that of a bare substrate to find the optical density due to the PF film alone. An estimate of the error in the film optical density was also made. With the film optical density found for light polarized parallel and perpendicular to the **z** axis, the dichroic ratio could then be calculated via eq 14.

Polarized fluorescence (PL) measurements were made using a Jobin-Yvon Fluoromax fluorimeter with Glan-Thomson polarizers inserted into the excitation and emission beams. The polarization bias of the instrument was taken into account.

X-ray Diffraction Measurements. GIXD measurements were performed at the W1.1 (ROEWI) beamline at HASYLAB in Hamburg. The beam was monochromatized by a double crystal Si(111) monochromator, and the X-ray energy was 8.8 keV. The beam was focused at the sample position, and the resulting beam size in the experimental hutch was 0.5 mm vertically and 4 mm horizontally. The samples were mounted onto the diffractometer by means of two translations and a horizontal tilt axis. Scattering of air and the risk of radiation damage were reduced by a helium atmosphere.

In GIXD, the incident angle range varied from 0.09° to 0.15° so that the penetration depth was small and the Bragg reflections due to the PI substrate were suppressed. In the measurement geometry (cf. Figure 4), the **x** axis is defined normal to the surface and **y** and **z** axes parallel to surface with **z** coinciding with the rubbing direction of the PI (cf. Figure 3). The GIXD patterns were measured with the incident beam along the **y** and **z** axes, respectively. The 1D intensity was measured with a scintillation counter and 2D intensity with an image plate (Molecular Dynamics), and for normalization, the incident flux was measured with an ionization chamber. The crystallite size (coherence length) has been estimated using a Scherrer formula, $L \cong \lambda/(\Delta 2\theta \cos\theta)$, where 2θ is the scattering angle, and the 1D intensities for which the instrumental function were assumed to be negligible. The Born approximation was regarded valid except close to the critical angle.[41]

IV. Results and Discussion

Degree of Overall Alignment as a Function of Molecular Weight. The uniaxial alignment of PF2/6 on PI[42] has been probed e.g. using polarized EL by Grell et al.[21] (M_n = 127 and M_w = 210 kg/mol). Aligned 147/260-PF2/6 has been studied using electron diffraction by Lieser et al.[18] As the theory and dichroism can be easily connected (cf. section II) we studied the alignment using polarized photoabsorption over same M_n range as in bulk.[17] Although the samples show large polydispersity (Table 1), the wide M_n range makes the comparison relevant.

The first alignment guideline is the temperature. The orientation procedure depends of course on the position of T_g, and PF2/6 does not align in the glassy state ($<T_g$). We were not able to determine T_g in films but relied on the bulk phase diagram ($T_g \sim 80$ °C[17]). The presence of the surface promotes alignment of the molecules and, therefore, may shift the T_g. However, for this effect to be sound, we should consider layers of the width comparable to a few molecular sizes.

Another paramount feature of the phase diagram[17] is the position of the Nem fluid regime as a function of M_n: At lower T, at glassy state or just above T_g the Nem−Hex transition is seen at $M_n^* = 10^4$ g/mol (cf. eq 4) separating LMW (Nem) and HMW (Hex) materials. For HMW compounds the Hex−Nem transition is observed to be at 140−165 °C for increasing M_n. The first and foremost guideline for alignment is thus to anneal LMW materials up to T_g (>80 °C) and the HMW samples up to the Nem−Hex transition (>165 °C). Consequently, to study the alignment as a function of M_n, the temperatures 80 and 180 °C were selected here for all M_n to probe the influence of phase domains.

The second alignment guideline addresses the annealing time. Because our theoretical treatment (ref 17 and section II) represents equilibrium statistical mechanics, we cannot give any prediction about the time scales involved. Therefore, to probe the degree of alignment as a function of M_n the annealing times were screened experimentally to see when the system approaches equilibrium, i.e., when the degree of alignment saturates. Banach et al.[34] reported the orientation saturation times to be from 10 min to more than 10 h for F8BT for increasing M_n from 69 to 188 kg/mol. We have previously used annealing of 10 min[28] and 3 h[19] for 8/15-PF2/6 and 147/260-PF2/6, respectively. We find that the selected 18 h (cf. section III) is far longer than the time scale over which the samples safely achieve the maximum degree of alignment: The degree is not considerably improved even after much shorter times

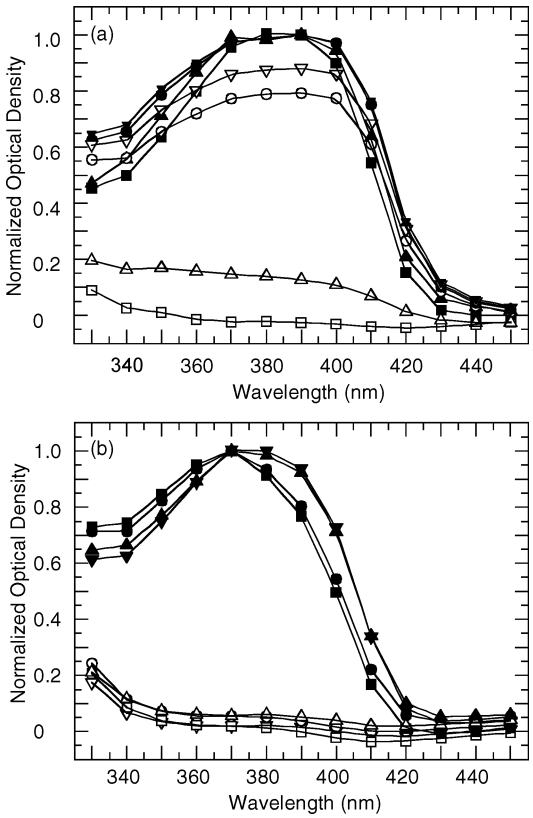

Figure 5. Polarized absorption spectra of (a) HMW and (b) LMW compounds. Open and solid symbols shows perpendicular and parallel components, respectively. 29/68-PF2/6 (squares), 62/138-PF2/6 (upper triangles), 92/190-PF2/6 (circles), and 147/260-PF2/6 (lower triangles) annealed at 180 °C for 18 h. (b) 3/5-PF2/6 (squares and circles), 8/15-PF2/6 (upper and lower triangles), annealed at 80 °C for 10 min or at 180 °C for 18 h, respectively. Data were interpolated by splines.

of 10 min and 3 h for LMW and HMW compounds, respectively. Therefore, we expect that our equilibrium theory is valid for the discussed experiment.

Figure 5 displays the polarized absorption spectra of aligned HMW compounds, when annealed at 180 °C for 18 h, and LMW compounds, when annealed at 80 °C for 10 min or at 180 °C for 18 h. Inspecting Figure 5a it is noteworthy that there is a large variation in dichroism for HMW samples depending on M_n despite the fact that all the samples have achieved Nem phase regime[17] during alignment process. Figure 5b shows in turn that the LMW samples align equally well when annealed just above T_g, at 80 °C for 10 min or at 180 °C for 18 h, which supports the assumption of the achieved equilibrium.

Figure 6 sums up the results of Figure 5, showing R after alignment as a function of M_n when two different annealing processes have been employed. The three heaviest samples did not align at 80 °C at all, so R was not determined. Table 2 depicts s and Ω (cf. section II) as a function of M_n for the discussed alignment procedures. The following conclusions can be drawn: LMW Nem samples align well above T_g. LMW samples do not align significantly better using either higher temperature or longer annealing time, which suggests that they reach the maximum degree of alignment at 80 °C in 10 min. With increasing M_n the degree of alignment for LMW samples increases. We have only two different M_n, but this effect is qualitatively very clear on the basis of several experiments and parallel samples. Then, HMW samples do not align or align very badly just above the

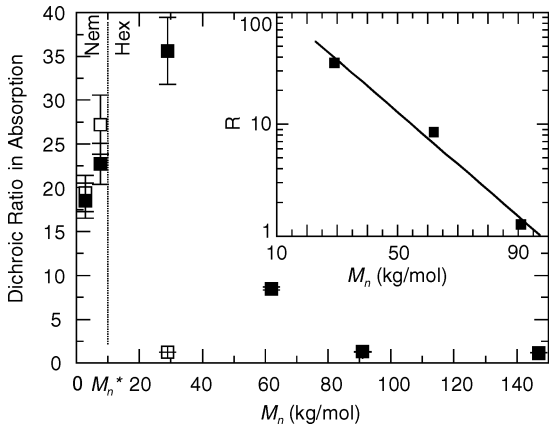

Figure 6. Dichroic ratios in absorption (R) as a function of M_n as measured at 380 nm. The open squares correspond to the samples annealed at 80 °C for 10 min and the solid squares those at 180 °C for 18 h A dotted line shows M_n*, the Nem−Hex transition point of PF2/6.[17] An inset shows the region of an exponential drop between $M_n = 10^4$ and 10^5 g/mol and a linear fit.

T_g, although they are plasticized. Instead, they align well when the alignment has been carried out at the Nem state above the Hex−Nem transition. The alignment of HMW samples at the Nem state does not fully occur in 10 min, but 3 h time considerably increases R which is saturated after that. It is very conspicuous that, in contrast to the LMW samples, increasing M_n *decreases* the degree of alignment for HMW compounds. In fact, R seems to drop exponentially, as depicted in the inset in Figure 6.

Thus, the overall picture for the alignment under virtually similar conditions, i.e., at the Nem phase regime, is that the degree of alignment first increases (R maybe linear) and then drops (R maybe exponential) when M_n is increased. So LMW samples behave quite differently compared to the HMW samples, not only in terms of self-assembly[17] but also in overall alignment. Furthermore, the maximum degree of alignment as a function of M_n is achieved at the boundary of these regimes, i.e., at around $M_n^* \sim 10^4$ g/mol, a fact which shows the usefulness of this parameter.[17] Note that in the first part of section II we assume that both phases show quite high degrees of orientational order, and here we actually see that this is a quite good approximation for not too high M_n.

The observation that PF2/6 aligns better in the Nem than in the Hex phase is obviously connected to the fact that the hexagonally packed molecules do not have the translational freedom to rearrange themselves as Nem molecules do. The Hex phase is much more viscous and can stick in metastable packing, a phenomenon which cannot be described in the framework of a simple equilibrium approach of section II. As discussed by Banach et al.[34] in the case of F8BT, the increasing viscosity may not allow R to saturate during reasonable observation times.

When we look on the degree of alignment of PF2/6 in the Nem phase as a function of M_n, then the obtained aligned regimes are interpreted as follows:

First, for small M_n the order parameter s should initially increase as a function of M_n mainly through the molecules that are no longer than 10 Kuhn segments as an order of magnitude. These molecules can be understood as simple LCs as described by Onsager theory.[39] Usually $\Omega_N \geq \Omega_H$ as far as the low M_n LCs

Table 2. Estimation of Order Parameter *s* and Solid Angle Accessible for the Direction Oscillations of PF2/6 as a Function of M_n

material	phase low *T*/high *T*	annealed at 80 °C for 10 min		annealed at 180 °C for 18 h	
		s	$\Omega/4\pi$	*s*	$\Omega/4\pi$
3/5-PF2/6	Nem	0.85 ± 0.01	0.10 ± 0.01	0.85 ± 0.02	0.10 ± 0.01
8/15-PF2/6	Nem	0.90 ± 0.01	0.07 ± 0.01	0.88 ± 0.02	0.08 ± 0.01
29/68-PF2/6	Hex/Nem	0.08 ± 0.01	0.87 ± 0.02	0.92 ± 0.02	0.05 ± 0.01
62/138-PF2/6	Hex/Nem			0.71 ± 0.02	0.21 ± 0.01
92/190-PF2/6	Hex/Nem			0.08 ± 0.01	0.89 ± 0.02
147/260-PF2/6	Hex/Nem			0.04 ± 0.01	0.92 ± 0.02

are concerned, and *s* (for a fixed molecule length) in the vicinity of the transition is about 10% higher in the smectic phase.[43] The persistence length of PF2/6 is measured to be around 7 nm.[44] As the lengths of molecules in the LMW regime are approximately twice of this, flexibility likely does not dominate. This is not the regime we consider in section II and our previous work.[17] We shall denote the small M_n LC regime, regime 1.

Second, for large M_n, i.e., for the HMW regime, the flexibility becomes important. If not flexible, the molecules in the melt would align perfectly apart from thermal fluctuations that would destroy the perfect overall order, and we could expect *s* to be very close to 1. If we look at the values of *s* just on the onset of the HMW regime, i.e., where *R* stops growing and starts decreasing, we find $R \sim 20-30$ and $s \sim 0.86-0.91$ (Table 2). As predicted by our theory in section II, the flexibility changes Ω. We note, in particular, that the scaling $\Omega \sim (\text{const})^{M_n}$ is predicted by eq 7. Thus, as far as eq 12 holds and $R = (1 + 2s)/(1 - s)$, we expect to see an exponential increase in Ω that implies an exponential decay in *R*. We stress that this is indeed observed in our experiment between $M_n = 10^4$ and 10^5 g/mol and presented in the inset of Figure 6. This M_n interval represents regime 2.

Third, we find that for $M_n > M_n^*$ *R* reaches its minimum (i.e., it cannot decrease further from unity), describing the tentative regime 3. Nonetheless, taking the small number of samples, we cannot make a clear distinction between regimes 2 and 3. It is noteworthy that although we discuss the alignment in the Nem phase, the same holds for the Hex phase with one exception. As described in ref 17, there is no regime 1 because there is no Hex phase for small PF2/6 molecules, i.e., for $M_n < M_n^*$.

For comparison, we made PL measurements to monitor film orientation as well as possible film degradation via the formation of keto defects (cf. Hintschich et al.[45]). Figure 7 shows typical polarized PL spectra of uniaxially aligned 8/15-PF2/6, indicating characteristic PL of PF2/6 and no major degradation. The difference is due to alignment and thus the polarization of PL, while the PL itself is not altered. The PL spectra of LMW compounds are similar to those of HMW materials.

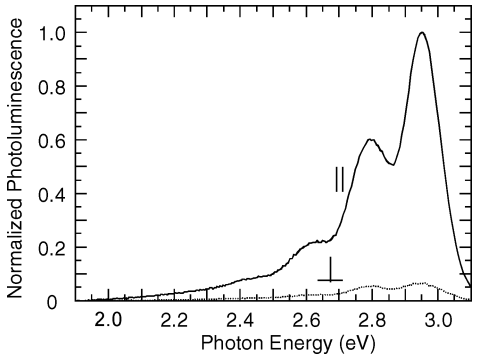

Figure 7. Polarized PL spectra of 8/15-PF2/6. The excitation light was polarized along the **z** axis, and the solid and dotted lines display the parallel and perpendicular PL component with respect to the **z** axis, respectively.

Self-Organized Structure Formation as a Function of Molecular Weight. *Hexagonal Multiple Oriented Films.* Depending on M_n, PF2/6 reveals Nem or Hex phases in bulk and in fibers.[17] Unlike in fibers, in thin films the unit cells of 147/260-PF2/6 are not hexagonal but, probably because of stress, marginally flattened (∼1.4%) in the **x** direction.[19] Although the structure might be denoted as orthogonal or pseudohexagonal, we still continue to call it hexagonal as the distinction between the theoretical Hex and Nem phases may be clearer. Most importantly, the GIXD results reveal two types of coexistent crystallites as illustrated in Figure 8.

We observed previously that the existence of two crystallite types is related to the decreased overall alignment of 147/260-PF2/6 compared to that of 8/15-PF2/6, but we were not able to clarify this in detail.[27] Banach et al.[34] observed that the alignment of higher M_n F8BT on PI was limited by the macroscopic multidomain structure, and we can ask whether the multiple orientation is a limiting factor of alignment. Both 147/260-PF2/6 and 29/68-PF2/6 takes on the Hex phase in bulk.[17] In this paper we find that 29/68-PF2/6 is well-aligned, actually *better* aligned than LMW polymers (cf. Table 2). Therefore, attention is first focused on the thin film structure of 29/68-PF2/6.

Figures 9 and 10 show GIXD patterns of highly ordered 29/68-PF2/6 on quartz and highly ordered *and* highly aligned 29/68-PF2/6 on PI, respectively. Both samples are annealed at 180 °C for 3 h, and *both* samples reveal the existence of two types of crystallites corresponding to Figure 8. Therefore, we find that both the in-plane (i.e., not uniaxially) aligned sample on quartz and the unixially well-aligned 29/62-PF2/6 on PI show two types of crystallites. This puts forward the assumption that the multiple-orientation phenomenon of the Hex phase is a surface effect and not crucially related to the chemical character of PI or the degree of unixial alignment.

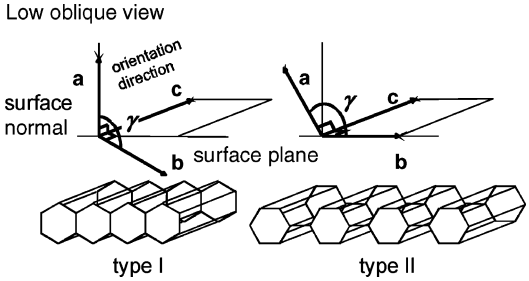

Figure 8. Schematics of the multiple orientation, "triaxial alignment": The mutual orientation of the orientation types I and II of hexagonal-like cells of PF2/6 with respect to the surface plane.

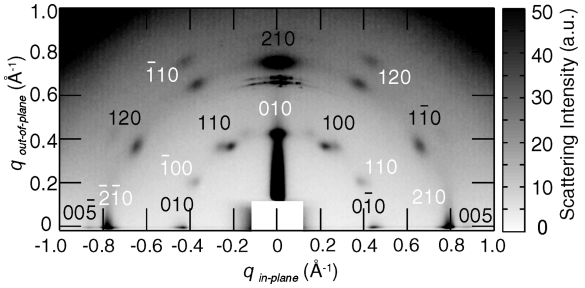

Figure 9. 2D GIXD patterns of the 29/68-PF2/6 film on quartz. Black and white indices correspond to types I and II, respectively (cf. Figure 8). The sharp out-of-plane arcs at ~0.65 Å^{-1} are not due to the sample.

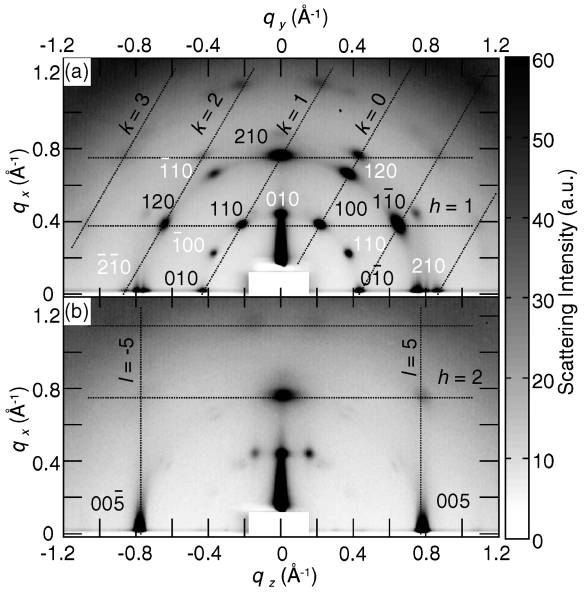

Figure 10. 2D GIXD patterns of the 29/68-PF2/6 film on PI. (a) (*xy*0) plane. (b) (*x*0*z*) plane. The dotted lines show a few reflection planes of type I. Black and white indices corresponds to the types I and II, respectively (cf. Figure 8). Reflection 210, which belongs to type I, is not in the same plane as reflections −110 and 120, which belong to type II.

All the HMW samples that reveal the Hex phase in bulk were then aligned using rubbed PI and annealed either at 80 °C for 10 min or 180 °C for 3 or 18 h. First, the HMW samples annealed at 180 °C show two types of crystallites whether they are well-aligned along the **z** axis or not. Thus, although we have previously found that this phenomenon is related to the low alignment of 147/260-PF2/6,[27] this relation does not hold for all M_n. The Hex phase is only able to retain a "single monodomain" on (00*c*) direction but not on (*ab*0) plane, and the multiple orientation may not be a simple reason or a consequence of decreased alignment. Second, the degree of alignment as a function of M_n varies in qualitative agreement with the optical result. The meridional GIXD data of samples for $M_n \geq 92$ kg/mol were contaminated by the equatorial peaks. Third, the samples annealed at 80 °C (i.e., not in Nem state) on PI are not aligned along the **z** axis but show Hex rather than disordered characteristics and two orientation types on the (*ab*0) plane. Fourth, both the alignment substrates (cf. Figure 4a,b) give identical GIXD characteristics (cf. Figure 11).

When putting forward an interpretation that the existence of the crystallite types is a surface effect, as it self-evidently is, but not related to the degree of

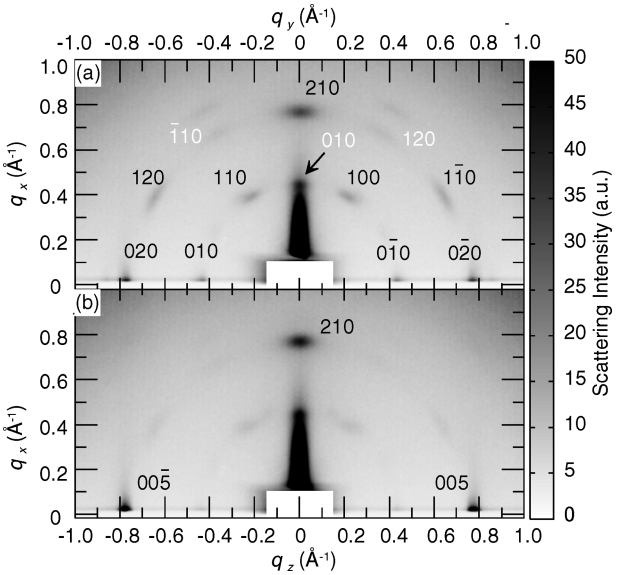

Figure 11. 2D GIXD patterns of 92/190-PF2/6 on Si/SiO_2/PI substrate spin-coated from 5 mg/mL solution. (a) (*xy*0) plane. (b) (*x*0*z*) plane. The black indices show primary reflections of orientation type I and white indices belong to those of type II. The proportion between the intensities of the types is roughly 2.5.

alignment, the question of the thickness related distribution of the types I and II arises. The multiple orientation of PATs[2] has not been studied as a function of thickness, but Banach et al.[34] observed that the domains of F8BT are distributed in-plane. We have previously suggested that the multiple orientation in PF2/6 is dependent on film thickness[19] and assumed that the crystallites are distributed out-of-plane rather than in-plane. Figure 11 shows the GIXD patterns of less aligned 92/190-PF2/6 when 5 mg/mL instead of 10 mg/mL solution is used, i.e., when the layer is thinner. The orientation is improved compared to the thicker film, yet the film reveals triaxial characteristics. Type I is dominant, and the intensity ratio between types I and II is roughly constant, around 3, when determined using the 100 reflection.

Figure 12a shows the dependence of the primary GIX reflections of the orientation types I and II as a function of the incident angle θ_i. The data were scanned with a 1D detector on the (*ab*0) plane, corresponding to angular directions 30°, 60°, 120°, and 150° in the 2D data shown in Figure 10, but with the different incident angle. The integrated intensity of the 100 and 110 reflections for both types (scaled to unity at $\theta_i = 0.18°$) behave the same way, showing primarily the onset of scattering at the critical angle where the penetration depth of the beam (Λ) increases rapidly to a few tens of micrometers (see Figure 12b). As the penetration depth of the beam below the critical angle (θ_c) is assumed to be around 100 Å[41] but the film thickness is known to be around 500 Å,[27] the GIXD method is expected to be quite thickness sensitive around critical angle. We assume that the divergence of the beam is negligible. The dashed and dotted lines (Figure 12a) show the ratio of corresponding reflections of the two orientation types. Had these types been distributed out-of-plane, this ratio would have shown a stepwise change at the critical angle. As no such thing is observed, this seems to indicate that the types I and II are distributed in-plane or form an intermixture, contrary to our earlier assumption.[19] However, we consider only the existence of either out-

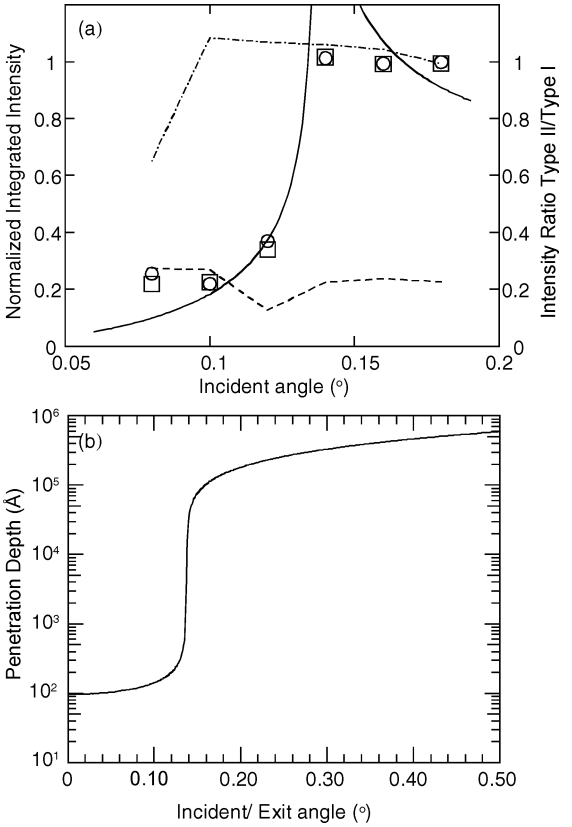

Figure 12. (a) Normalized average of the relative integrated intensities of 100 and 110 reflections of the orientation types I (open spheres) and II (open squares), respectively, as a function of incident angle of the incoming radiation. The data correspond to the sample 29/68-PF2/6 (cf. Figure 11). The dashed and dashed and dotted lines show the absolute intensity rations of type II and I calculated using the 100 and 110 reflections, respectively. The solid line shows the expected dependence for the scattering intensity $\theta_i T(1 - \exp(D/\Lambda))$, where $\theta_i \ll \theta_c$ is the geometrical factor which gives the amount of flux incident on the sample surface (assuming that the whole surface is still totally within the beam at $\theta_i = 0.2°$), $T = 1 - R$ is the transmission factor of the ideally smooth PF2/6 surface, $D = 500$ Å is the thickness of the scattering layer, and $\Lambda = 65$ Å is the penetration depth. (b) Calculated penetration depth (Λ) (either incident or out-going) for PF2/6 and 8.8 keV.

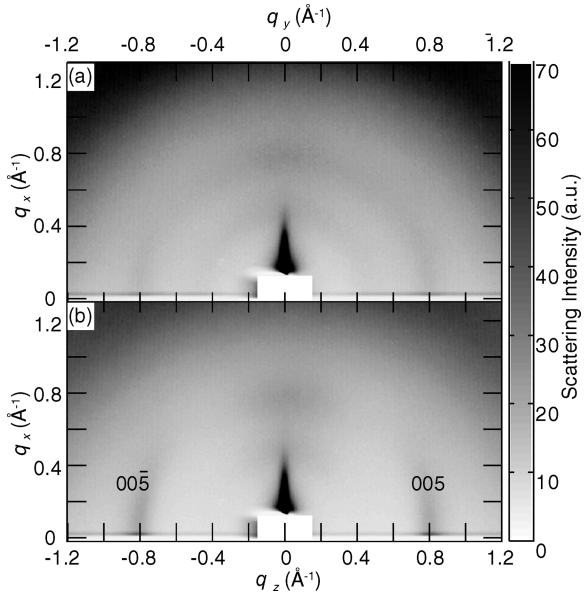

Figure 13. 2D GIXD patterns of 3/5-PF2/6 film: (a) (xy0) plane; (b) (x0z) plane.

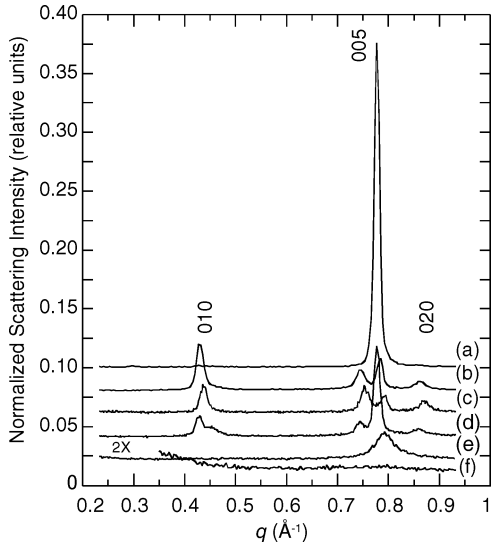

Figure 14. 1D GIXD scans illustrating the change of local order in films when passing the Nem−Hex transition. 29/68-PF2/6 on rubbed PI: (a) In-plane, incoming beam along the **y** axis. (b) In-plane and (c) out-of-plane, incoming beam along the along the **z** axis. (d) In-plane scan on similarly annealed 29/68-PF2/6 on quartz. 8/15-PF2/6 on rubbed PI: (e) In-plane, incoming beam along the **y** axis. (f) Out-of-plane, incoming beam along the **z** axis. The samples were annealed at 180 °C for 3 h.

of-plane or in-plane distribution, and we cannot exclude the possibility of more complicated texture. Note further that the multiple orientation is still a thin film property; the out-of-plane distribution must arise when increasing the thickness of the film up to the level of a fiber (i.e., tens of microns).

Nematic Films. In bulk,[17] Nem rather than a Hex phase is seen generally for $M_n < M_n$*. The used materials exhibit quite large polydispersity (Table 1), and therefore 8/15-PF2/6 shows occasionally traces of hexagonal XRD patterns in bulk.[17] However, they are never seen in films. Figure 13 shows in turn GIXD patterns of 3/5-PF2/6, also indicating uniaxially well-aligned Nem structure. Despite the short backbone, 3/5-PF2/6 "decamer" reveals clear 005 GIX reflections in films, indicating the 5-helical hairy-rod-like structure, an indirect assumption of the theory.[17] All in all, although HMW polymers reveal a significant difference between bulk and film on PI, the local structure of LMW samples in aligned films on PI corresponds to that in bulk. In agreement with the optical dichroism, there is no difference in orientation between the LMW samples annealed at 80 or 180 °C.

Local Order of Hexagonal and Nematic Films. We report on the high coherence length ($L \sim 300$ Å) of PF2/6 in bulk in ref 17. Although the crystallite size is quite dependent on the thermal history, the distinction in the local order between different cases may be studied. Figure 14 presents the 1D GIXD scans of the Hex and Nem samples just above and below the limit M_n* at room temperature. The local order in highly aligned multiple-oriented Hex 29/68-PF2/6 (Figure 14a−c) is very high, 610 Å in the meridional direction when measured by the 005 reflection at 0.78 Å^{-1}, 230 Å on the (ab0) plane when measured by the 010 (type I) reflection at 0.43 Å^{-1}, and 250 Å when measured by 010

(type II) reflection at 0.44 Å^{-1}. The 29/68-PF2/6 on quartz (Figure 14d) gives the corresponding values 270 Å (0.78 Å^{-1}) and 170 Å (0.43 Å^{-1}). Unsurprisingly, Nem 8/15-PF2/6 (Figure 14e) gives considerably lower values ~80 Å (0.79 Å^{-1}) that may vary up to 100 Å depending on the sample.

As expected, the difference between the Nem and Hex samples is overwhelming. Further, in all cases the local order is better along the **c** axis than in the (ab0) plane. Then, interestingly, uniaxially aligned samples, whether Nem or Hex, seem to show higher L compared to those aligned in-plane or bulk,[17] Figure 14a−d representing a particular example. As noted above, if Hex samples are annealed at 80 °C for 10 min, clear hexagonal GIXD patterns are obtained, but the material is not, or only slightly, aligned. In such case L seems still to be quite high, 270−280 Å, measured via the 005 reflection, but not that high as in the case of well-aligned samples. The aligned PF2/6 may pack better showing increased local order as well. It is not only the alignment and multiple orientation but also the local order which is affected by the film environment compared to the bulk phase.

V. Conclusions

A systematic study of the influence of M_n on the thermotropic alignment and structure of PF2/6 hairy rods in the anisotropic thin film on rubbed PI has been conducted in equilibrium. This polymer has been selected as a simple "model" hairy rod and simultaneously as a useful polymer for in thin film devices. The alignment of PF2/6 was studied using polarized photoabsorption and compared to the theoretical predictions while the structure was studied using GIXD. The experiments have been discussed in the terms of the theory presented here. The phase behavior in bulk[17] has been used to optimize the local order and alignment conditions. The differences between bulk and film have been highlighted.

In line with the bulk behavior,[17] we find a threshold molecular weight $M_n^* = 10^4$ g/mol separating two regimes: LMW ($M_n < M_n^*$) and HMW ($M_n > M_n^*$). The orientational order of these materials was allowed to saturate by annealing LMW materials for 10 min at 80 °C and HMW materials for 18 h at 180 °C, justifying the use of equilibrium statistical mechanics. The aligned polymer chains are parallel to the substrate in the **z** direction, corresponding to the rubbing direction of PI. The orientational order is maximized near the boundary of the regimes, i.e., when $M_n \sim M_n^*$. The orientational order parameter s gets values >0.9.

LMW samples align almost equally well at any $T > T_g$, and the orientational order *increases* with M_n. In agreement with the bulk results,[17] LMW materials are interpreted as obeying the theory of small M_n LCs for which the flexibility is not dominant. In agreement with the bulk, the Nem 5-helical structure has been found for LMW materials. The LMW samples show no distinct order in the (ab0) plane, and a meridional coherence length is less than 100 Å.

HMW compounds do not align in the Hex phase but align well in the Nem phase, when the temperature is raised above the Hex−Nem transition that is at 140−170 °C depending on M_n. This is understood to be due to the more limited translational freedom and the metastable packing of the Hex phase. For HMW compounds the dichroic ratio R *decreases* exponentially with M_n. This is predicted by theory and confirmed by experiment for $M_n = 10^4-10^5$ g/mol. R seems to saturate for $M_n \geq 10^5$ g/mol. All HMW materials—whether unixially aligned or not—reveal two kinds of coexistent crystallites, "triaxial" alignment, where the greater proportion of the crystallites have one crystal axis **a** perpendicular and smaller proportion parallel to the substrate surface. These types are distributed in-plane. This multiple orientation phenomenon is not directly related to the lower degree of alignment. The Hex phase has been found to be locally highly ordered, revealing a coherence length characteristically 250 Å on the (ab0) plane and more than 600 Å along the (00c) direction surpassing the local order of unaligned similarly annealed HMW film on quartz or bulk HMW materials.[17] For all cases, meridional order seems higher than equatorial, and no large difference between orientation types has been observed. Importantly, the sample showing the highest s, $M_n = 29$ kg/mol, shows simultaneously the highest degree of local order and reveals a multiple oriented Hex phase in films.

Acknowledgment. This study has been funded by One North-East (UK) UIC nanotechnology grant. B.P.L. receives a CASE studentship from Sony Europe Ltd. M.K. acknowledges the Jenny and Antti Wihuri Foundation and Academy of Finland for support and Prof. M. J. Winokur of the University of Wisconsin—Madison for notes and access to the unpublished results.

References and Notes

(1) Winokur, M. J. Structural Studies of Conducting Polymers. In *Handbook of Conducting Polymers*; Skotheim, T. A., Elsenbaumer, R. L., Reynolds, J. R., Eds.; Marcel Dekker: New York, 1998; pp 707−726.
(2) Sirringhaus, H.; Brown, P. J.; Friend, R. H.; Nielsen, M. M.; Bechgaard, K.; Langeveld-Voss, B. M. W.; Spiering, A. J. H.; Janssen, R. A. J.; Meijer, E. W.; Herwig, P.; de Leeuw, D. M. *Nature (London)* **1999**, *401*, 685−688.
(3) Aasmundtveit, K. E.; Samuelsen, E. J.; Guldstein, M.; Steinsland, C.; Flornes, O.; Fagermo, C.; Seeberg, T. M.; Pettersson, L. A. A.; Inganäs, O.; Feidenhans'l, R.; Ferrer, S. *Macromolecules* **2000**, *33*, 3120−3127.
(4) Winokur, M. J.; Chunwachirasiri, W. *J. Polym. Sci., Part B: Polym. Phys.* **2003**, *41*, 2630−2648.
(5) Ballauff, M. *Macromolecules* **1986**, *19*, 1366−1374.
(6) Ballauff, M. *J. Polym. Sci., Part B: Polym. Phys.* **1987**, *25*, 739−747.
(7) Ballauff, M. *Angew. Chem., Int. Ed. Engl.* **1989**, *101*, 261−276.
(8) Samuelsen, E. J.; Mårdalen, J. The Structure of Polythiophenes. In *Handbook of Organic Conductive Molecules and Polymers*; Nalwa, H. S., Ed.; Wiley: New York, 1997; Vol. 3, pp 87−120.
(9) Scherf, U.; List, E. J. W. *Adv. Mater.* **2002**, *14*, 477−487.
(10) Grell, M.; Bradley, D. D. C. *Adv. Mater.* **1999**, *11*, 895−905.
(11) Sirringhaus, H.; Wilson, R. J.; Friend, R. H.; Inbasekaran, M.; Wu, W.; Woo, E. P.; Grell, M.; Bradley, D. D. C. *Appl. Phys. Lett.* **2000**, *77*, 406−408.
(12) Kinder, L.; Kanicki, J.; Swensen, J.; Petroff, P. *Proc. SPIE Int. Soc. Opt. Eng.* **2003**, *5217*, 35−42.
(13) Kawana, S.; Durrell, M.; Lu, J.; MacDonald, J. E.; Grell, M.; Bradley, D. D. C.; Jukes, P. C.; Jones, R. A. L.; Bennett, S. L. *Polymer* **2002**, *43*, 1907−1913.
(14) Surin, M.; Hennebicq, E.; Ego, C.; Marsitzky, D.; Grimsdale, A. C.; Müllen, K.; Brédas, J.-L.; Lazzaroni, R.; Leclère, P. *Chem. Mater.* **2004**, *16*, 994−1001.
(15) Tanto, B.; Guha, S.; Martin, C. M.; Scherf, U.; Winokur, M. J. *Macromolecules* **2004**, *37*, 9438−9448.
(16) Nothofer, H.-G.; Meisel, A.; Miteva, T.; Neher, D.; Forster, M.; Oda, M.; Lieser, G.; Sainova, D.; Yasuda, A.; Lupo, D.; Knoll, W.; Scherf, U. *Macromol. Symp.* **2000**, *154*, 139−148.
(17) Knaapila, M.; Stepanyan, R.; Torkkeli, M.; Lyons, B. P.; Ikonen, T.; Almásy, L.; Foreman, J. P.; Serimaa, R.; Güntner, R.; Scherf, U.; Monkman, A. P. *Phys. Rev. E*, in press.

(18) Lieser, G.; Oda, M.; Miteva, T.; Meisel, A.; Nothofer, H.-G.; Scherf, U.; Neher, D. *Macromolecules* **2000**, *33*, 4490−4495.
(19) Knaapila, M.; Lyons, B. P.; Kisko, K.; Foreman, J. P.; Vainio, U.; Mihaylova, M.; Seeck, O. H.; Pålsson, L.-O.; Serimaa, R.; Torkkeli, M.; Monkman, A. P. *J. Phys. Chem. B* **2003**, *107*, 12425−12430.
(20) Wenzel, M.; Ballauff, M.; Wegner, G. *Makromol. Chem.* **1987**, *188*, 2865−2873.
(21) Grell, M.; Knoll, W.; Lupo, D.; Meisel, A.; Miteva, T.; Neher, D.; Nothofer, H.-G.; Scherf, U.; Yasuda, A. *Adv. Mater.* **1999**, *11*, 671−675.
(22) Miteva, T.; Meisel, A.; Nothofer, H.-G.; Scherf, U.; Knoll, W.; Neher, D.; Grell, M.; Lupo, D.; Yasuda, A. *Proc. SPIE Int. Soc. Opt. Eng.* **1999**, *3797*, 231−236.
(23) Meisel, A.; Miteva, T.; Glaser, G.; Scheumann, V.; Neher, D. *Polymer* **2002**, *43*, 5235−5242.
(24) Banach, M. J.; Friend, R. H.; Sirringhaus, H. *Macromolecules* **2004**, *37*, 6079−6085.
(25) Chen, D.; Winokur, M. J.; Masse, M. A.; Karasz, F. E. *Polymer* **1992**, *33*, 3116−3122.
(26) Prosa, T. J.; Winokur, M. J.; Moulton, J.; Smith, P.; Heeger, A. J. *Macromolecules* **1992**, *25*, 4364−4372.
(27) Knaapila, M.; Kisko, K.; Lyons, B. P.; Stepanyan, R.; Foreman, J. P.; Seeck, O. H.; Vainio, U.; Pålsson, L.-O.; Serimaa, R.; Torkkeli, M.; Monkman, A. P. *J. Phys. Chem. B* **2004**, *108*, 10711−10720.
(28) Lyons, B. P.; Monkman, A. P. *J. Appl. Phys.* **2004**, *96*, 4735−4741.
(29) Gitsas, A.; Floudas, G.; Wegner, G. *Phys. Rev. E* **2004**, *69*, 041802.
(30) Heffner, G. W.; Dahman, S. J.; Pearson, D. S.; Gettinger, C. L. *Polymer* **1993**, *34*, 3155−3159.
(31) Kline, J. R.; McGehee, M. D.; Kadnikova, E. N.; Liu, J.; Frechet, J. M. J. *Adv. Mater.* **2003**, *15*, 1519−1522.
(32) Zen, A.; Pflaum, J.; Hirschmann, S.; Zhuang, W.; Jaiser, F.; Asawapirom, U.; Rabe, J. P.; Scherf, U.; Neher, D. *Adv. Funct. Mater.* **2004**, *14*, 757−764.
(33) Papadopoulos, P.; Floudas, G.; Chi, C.; Wegner, G. *J. Chem. Phys.* **2004**, *120*, 2368−2374.
(34) Banach, M. J.; Friend, R. H.; Sirringhaus, H. *Macromolecules* **2003**, *36*, 2838−2844.
(35) Khokhlov, A. R.; Semenov, A. N. *Physica A* **1982**, *112*, 605−614.
(36) Stepanyan, R.; Subbotin, A.; Knaapila, M.; Ikkala, O.; ten Brinke, G. *Macromolecules* **2003**, *36*, 3758−3763.
(37) Subbotin, A.; Stepanyan, R.; Knaapila, M.; Ikkala, O.; ten Brinke, G. *Eur. Phys. J. E* **2003**, *12*, 333−345.
(38) Semenov, A. N.; Khokhlov, A. R. *Statistical Physics of Liquid-Crystalline Polymers*; *Sov. Phys. Usp.* **1988,** *156*, 427−476.
(39) Khokhlov, A. R. Theories based on the Onsager approach. In *Liquid Crystallinity in Polymers*; Ciferri, A., Ed.; VCH Publishers: New York, 1991; pp 97−129.
(40) de Gennes, P. G.; Prost, J. *The Physics of Liquid Crystals*, 2nd ed.; Oxford University Press: Oxford, 1998.
(41) Dosch, H. Critical Phenomena at Surfaces and Interfaces. In *Springer Tracts in Modern Physics*; Hoehler, G., Ed.; Springer-Verlag: Berlin, 1992; Vol. 126.
(42) Bauer, C.; Urbasch, G.; Giessen, H.; Meisel, A.; Nothofer, H.-G.; Neher, D.; Scherf, U.; Mahrt, R. F. *ChemPhysChem* **2000**, *1*, 142−146.
(43) McMillan, W. L. *Phys. Rev. A* **1971**, *4*, 1238−1246.
(44) Fytas, G.; Nothofer, H. G.; Scherf, U.; Vlassopoulos, D.; Meier, G. *Macromolecules* **2002**, *35*, 481−488.
(45) Hintschich, S. I.; Rothe, C.; Sinha, S.; Monkman, A. P.; Scandiucci de Freitas, P.; Scherf, U. *J. Chem. Phys.* **2003**, *119*, 12017−12022.

MA0477403